

**NO oxidation properties of Pt(111) revealed by *ab initio* kinetic simulations**S. Ovesson,<sup>1</sup> B. I. Lundqvist,<sup>1</sup> W. F. Schneider,<sup>2,\*</sup> and A. Bogicevic<sup>2</sup><sup>1</sup>*Department of Applied Physics, Chalmers University of Technology and Göteborg University, S-412 96 Göteborg, Sweden*<sup>2</sup>*Scientific Research Laboratories, Ford Motor Company, Dearborn, Michigan 48124, USA*

(Received 9 August 2004; published 9 March 2005)

As a well-known oxidation catalyst, platinum is currently being used to convert NO to NO<sub>2</sub> for absorption in so-called NO<sub>x</sub> traps under excess oxygen conditions, where direct conversion of NO to nitrogen gas is prohibitive. By performing kinetic Monte Carlo simulations with parameters derived from density-functional theory, we show that this oxidation process is not an inherent property of the platinum catalyst itself. In fact, the intrinsic NO+O→NO<sub>2</sub> reaction is found to be inhibited (endothermic) rather than promoted on Pt(111), due to strong oxygen-platinum bonds. Only at sufficient oxygen chemical potential does platinum become an efficient oxidation catalyst, as its oxygen bonds are weakened with increasing coverage, and the NO<sub>2</sub> formation reaction becomes exothermic. At that point, Pt catalyzes the reaction by lowering the activation barrier for the kinetic reaction. Congruent with flow-reactor experiments, we note a strong temperature dependence for the turnover frequency, which should encourage further ultra-high vacuum studies.

DOI: 10.1103/PhysRevB.71.115406

PACS number(s): 68.43.Bc, 68.43.Jk, 82.65.+r

**I. INTRODUCTION**

Increasingly more stringent emissions and fuel economy requirements have spurred the introduction of lean-burn gasoline and diesel engines, in which hydrocarbons are combusted in excess (above stoichiometric) atmosphere of oxygen.<sup>1</sup> Conventional three-way catalysts, which operate very well in traditional powertrains, are unfortunately ineffective in removing nitrogen oxides (NO<sub>x</sub>,  $x=1-2$ ) from the exhaust gas under such conditions. One way around this predicament is to induce selective catalytic reduction of NO<sub>x</sub> by means of injection of urea or some other reductant into the catalytic converter.<sup>2,3</sup> Another approach which has gained considerable attention is the temporary chemical trapping of NO<sub>x</sub> under lean conditions and subsequent release during brief excursions to reducing (fuel-rich) conditions.<sup>4,5</sup> Both approaches rely fundamentally on the ability to catalytically oxidize NO, the primary component of NO<sub>x</sub> from the combustion process, into NO<sub>2</sub>. Typically, noble-metal catalysts are used for this purpose, but it is presently unclear as to what limits their activity and how they interact with the oxide supports. Theoretical investigations have traditionally been performed using first-principles or simpler semi-empirical molecular modeling. The former approach provides energetics and reaction barriers with chemical accuracy, while the latter lacks such accuracy but instead provides a probe into more relevant size and time scales. Here we present a hybrid approach that combines the advantages of either method, providing significant new insight into the oxidation reaction and the means to separate intrinsic catalytic properties from the effects of varying thermodynamic conditions.

In heterogeneous catalysis, reaction rates for the formation of chemical bonds are seldom just diffusion limited, and the reaction kinetics therefore often depend on residence times in precursor states that are very sensitive to adsorbate interactions. A theory aiming to quantitatively assess complex reaction kinetics must be able to take into account these

effects over relevant time and length scales. The magnitude and extent of both direct and indirect adsorbate interactions have been studied previously.<sup>6-8</sup> In the present work, such interactions are quantified from first principles for a three-component system and incorporated into our simulations. Extending the realm of first-principles investigations from the time and length scales of atom dynamics to those of technologically relevant chemical processes like epitaxial growth and catalytic reactions always represents an outstanding challenge. A computationally intensive but quite useful approach is to combine density-functional theory (DFT) and kinetic Monte Carlo (KMC) simulations. This methodology has been exemplified in several recent studies of epitaxial growth of single-component metal and semiconductor systems.<sup>9-12</sup> Because this approach requires an extensive mapping of the elementary processes involved and an accurate calculation of their activation energies, it has yet to make an instep into even more complex areas like catalysis.

In this paper, we present a successful generalization of the DFT-KMC method to a catalytic reaction: the oxidation of NO on Pt(111). The study encompasses a detailed assessment of the energetics, mass transport, and reaction kinetics of O, NO, and NO<sub>2</sub> over Pt(111). The main result is the determining role the oxygen coverage plays in determining the direction of the NO oxidation reaction. To assess the feasibility of using simpler pairwise models for studying systems of this complexity, we also perform a detailed analysis of lateral adsorbate interactions.

**II. COMPUTATIONAL DETAILS**

As in all KMC simulations, it is important to first determine what elementary processes, here diffusion, reaction, and desorption steps, are likely to be important in the reaction process. By combining existing data on surface intermediates with detailed balance and chemical intuition, we have deduced a list of salient reactions, further discussed below.

TABLE I. Adsorption energies  $E_a$  in eV and adsorption heights  $d_a$  in Å above the plane averaged over all surface atoms with five (5L) and four (4L) surface layers, respectively.

	$E_a^{5L}$	$E_a^{4L}$	$d_a^{5L}$	$d_a^{4L}$
N	4.72	4.69	1.00	1.00
O	4.39	4.36	1.16	1.13
NO	1.44	1.28	1.92	1.89
NO <sub>2</sub> <sup>(i)</sup>	1.44	1.28	2.36	2.35
NO <sub>2</sub> <sup>(ii)</sup>	1.34	1.24	2.59	2.58
NO <sub>2</sub> <sup>(iii)</sup>	1.34	1.23	2.58	2.61
NO <sub>2</sub> <sup>(iv)</sup>	1.36	1.20	2.40	2.43

The rate of each reaction (including adsorption, diffusion, and desorption) is calculated within transition-state theory using DFT-derived activation energies. The DFT calculations encompass a supercell plane wave pseudopotential method within the PW91 implementation of the generalized gradient approximation (GGA).<sup>13,14</sup> The computational details are described in Ref. 15, unless otherwise noted. The supercells are constructed of four  $4 \times 4$  (111) Pt layers, the top two of which are fully relaxed and the other two frozen at bulk crystal positions, and five vacuum layers, and the Brillouin zone is sampled with a uniform  $3 \times 3$   $\mathbf{k}$ -point mesh.

Transition states for the diffusion and reaction processes are calculated with the nudged elastic band (NEB) method,<sup>16</sup> with four system replicas used between initial- and final-state geometries to achieve a smooth minimum-energy path upon relaxation, determining the activation energies via spline fits. For adsorbate diffusion (O, NO), the transition states are quite simple, located near the geometric saddle points, while for surface-mediated chemical reactions, the minimum-energy paths and transition states are highly complex, as described further below.

### III. ADSORPTION ENERGETICS

On the Pt(111) surface, O and NO have previously been shown to adsorb preferentially at fcc threefold hollow sites, the latter N-down and normal to the surface.<sup>15,17</sup> The calculated adsorption energies at  $\Theta=1/16$  monolayer (ML) (where unit coverage is defined as one adsorbate per surface Pt atom), using the four-layer slab model (Table I), correspond well with previous calculations at  $\Theta=1/9$  ML,<sup>15</sup> using five-layer slabs. A supercell with four substrate layers is thus deemed sufficiently accurate for the present purposes.

While the determination of the preferred O and NO adsorption structures is relatively straightforward, NO<sub>2</sub> adsorption is more complex and less well understood. Here we investigate a number of O-down, N-down, and NO-down NO<sub>2</sub> adsorption geometries oriented along the  $\langle 110 \rangle$ ,  $\langle 111 \rangle$ , and  $\langle 112 \rangle$  directions: (i) NO-down atop along  $\langle 110 \rangle$ , where the second O atom points up and away from the surface, (ii) N-down atop with two O atoms in bridge sites along  $\langle 110 \rangle$  toward the vacuum, (iii) N-down atop with the O atoms in fcc and hcp sites along  $\langle 112 \rangle$ , and (iv) the O atoms down in

TABLE II. Interaction energies in eV and interaction-induced relaxations in Å for O, NO, and NO<sub>2</sub> adsorbates on Pt(111). Interactions beyond 3-NN separation are ignored. Interaction energies  $E_{XY}^{\text{int}}$  are given in eV as  $E_{XY} + E_{\text{slab}} - E_X - E_Y$ , but reduced by 1/2 for third nearest neighbors to correct for periodic image interactions.  $d_{\text{rel}}$  is the amount of spatial repulsion induced by adsorbate interactions.

	1-NN		2-NN		3-NN
	$E^{\text{int}}$	$d_{\text{rel}}$	$E^{\text{int}}$	$d_{\text{rel}}$	$E^{\text{int}}$
N-N	0.36	0.30	0.09	0.02	0.04
O-O	0.20	0.20	0.10	0.02	0.02
NO-NO	0.31	0.24	0.12	-0.00	0.06
NO-O	0.24	0.22	0.10	0.03	0.03
O-NO <sub>2</sub> <sup>(i)</sup>	0.10	0.82	0.10	0.72	0.06
O-NO <sub>2</sub> <sup>(ii)</sup>	0.07	0.09	0.06	0.01	0.03
O-NO <sub>2</sub> <sup>(iii)</sup>	0.06	0.07	0.07	0.01	0.02
O-NO <sub>2</sub> <sup>(iv)</sup>	0.35	0.53	0.09	0.01	0.02

top sites along  $\langle 110 \rangle$  and N above in the bridge site in between. The minimum-energy geometry is (i) (shown in Fig. 1), conventionally labeled  $\mu$ -N,O-nitrito, in excellent agreement with HREELS data.<sup>18</sup>

The parameters used in the low-coverage KMC simulations for the rates of all the elementary processes, including diffusion, chemical reactions, and desorption, are computed within DFT (Table II). A common prefactor of  $10^{13}$  Hz is adopted for all processes. A rigorous computation of the diffusion prefactor from first principles and transition-state theory<sup>19</sup> gives values around  $10^{13}$  Hz. The general use of a value like this can be justified by noting that the rates depend exponentially on the activation energies and linearly on the prefactors. At the substrate temperatures considered in this study, prefactor variations of one to two orders of magnitude, which is at most what one expects, will still have a lesser impact on the reaction rates than the variations we expect from the small, but more important errors in our activation barriers.

### IV. PAIR INTERACTIONS

In the high O<sub>2</sub> concentrations characteristic of lean exhaust, a significant oxygen coverage of the noble metal is expected. The lateral NO-O interactions under such conditions are therefore of principal interest and call for quantification. Pair interaction energy values are here computed for interactions between O, NO, and NO<sub>2</sub> on Pt(111) (Table II). The adsorbates are kept in threefold fcc hollows unless otherwise noted, and the counting of neighbors is made with respect to the fcc lattice.

In first nearest-neighbor (1-NN) configurations, the interactions are generally repulsive and of the order of 0.2–0.3 eV (except O-NO<sub>2</sub>, see below), i.e., quite considerable. Already in next-nearest (2-NN) configurations, adsorbate interactions are much weaker, by a factor of 2–4, and in 3-NN configurations all interaction energies are less than or

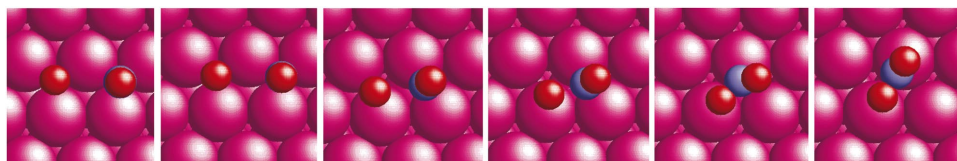


FIG. 1. (Color) Top view of the minimum-energy path for  $\text{NO}_2$  formation from  $\text{NO}$  and  $\text{O}$ , as computed within DFT-GGA and NEB. The  $\text{O}$  atoms are colored red and the  $\text{N}$  atom blue.

about 0.05 eV. The interaction-induced adsorbate relaxations are all found to be 0.2–0.3 Å at the shortest separations, but only a tenth of that for 2-NN.

For the  $\text{O}-\text{NO}_2$  entries, the designations 1-NN, 2-NN, etc., are made with respect to the fcc site closest to the  $\text{NO}_2$ , for which reason the interaction energies are not strictly comparable with those of the other molecule pairs. The important observation, however, is that the  $\text{O}-\text{NO}_2$  interactions are quite weak in all configurations, as expected, given the stability of  $\text{NO}_2$ .

If interactions beyond the 3-NN separation and many-body contributions can be neglected, the interaction energetics  $V_i^{XY}$ , i.e., the pair interaction energy for species  $X$  and  $Y$  at  $i$ th nearest-neighbor separation (Table II), determines the ground-state adsorbate patterning of the surface. For the  $\text{O}/\text{Pt}(111)$  system, the inequalities  $V_3 > 0$ ,  $V_1 > 3V_3$ , and  $V_2 > 2V_3$  hold, and the  $p(2 \times 2)$  structure is then predicted at  $\Theta = 25\%$ .<sup>20</sup>

This is in good agreement with experimental findings.<sup>21</sup>

### V. NO VS $\text{NO}_2$ STABILITY

In the gas phase, the reaction  $\text{NO} + 1/2\text{O}_2 \rightarrow \text{NO}_2$  is exothermic by 1.20 eV. On the clean  $\text{Pt}(111)$  surface, the  $\text{O}_2$  dissociates at 150 K,<sup>22</sup> and the oxidation reaction  $\text{NO} + \text{O} \rightarrow \text{NO}_2$  is instead *endothermic* by 0.7 eV. Thus *Pt(111) by itself does not catalyze NO oxidation!* However, with increasing  $\text{O}$  coverage the energetics is changed in favor of  $\text{NO}_2$ , due to strong repulsive  $\text{O}-\text{O}$  and  $\text{O}-\text{NO}$  interactions. The sample calculations presented in Fig. 2 and Table III illustrate this: For an  $\text{NO}$  in a saturated  $\text{O}$   $p(2 \times 2)$  overlayer (i.e., removing an  $\text{O}$  from the  $p(2 \times 2)$  structure to form  $\text{NO}_2$ , from configuration 12 to 13 in Fig. 2), the reaction is nearly isothermic. Increasing the initial  $\text{O}$  coverage (i.e., be-

fore adding  $\text{NO}$ ) to 5/16 (from configuration 14 to 15) the  $\text{NO}_2$  becomes favored by 0.28 eV.

It is thus clear that the  $\text{NO} \rightarrow \text{NO}_2$  conversion on  $\text{Pt}(111)$  is driven by lateral adsorbate interactions. To accurately predict the kinetic consequences of these interactions, one needs to explore a larger fraction of the full configuration space beyond the sample calculations displayed in Fig. 2. Reaction energetics and kinetics can both be assessed in KMC simulations if, in addition to clean-surface activation energies, the interaction energetics can be properly accounted for. Pairwise summation of interaction energies would be a tractable solution apt for KMC implementation.

Using the computed interaction energies (Table II), pairwise summation is performed for more complex adsorbate configurations. The expansion of the energy in terms of pair interactions is truncated at the 3-NN separation. The various configurations considered are displayed in Fig. 2, and the energies appear in Table III. Pairwise summation with 3-NN interactions works rather well, with errors smaller than 0.10 eV per atom even at the highest coverages and/or most frustrated geometries (i.e., those allowing the least lateral relaxation).

### VI. KINETICS OF NO OXIDATION

In order to assess the kinetic effects of lateral interactions and  $\text{O}$  coverage on the  $\text{NO} + \text{O} \rightarrow \text{NO}_2$  conversion in oxygen-rich environments, we perform a set of first-principles KMC simulations<sup>23</sup> of  $\text{NO}$  deposition on the  $\text{O}$ -precovered  $\text{Pt}(111)$  surface. The activation energies are calculated with DFT, as reported here and in Ref. 15

The relevant (i.e., not too rare) processes are  $\text{O}$  diffusion (activation energy=0.56 eV),  $\text{NO}$  diffusion [0.24 eV; diffusion barrier for  $\text{N}$  is found a little high (0.81 eV)],  $\text{NO}_2$

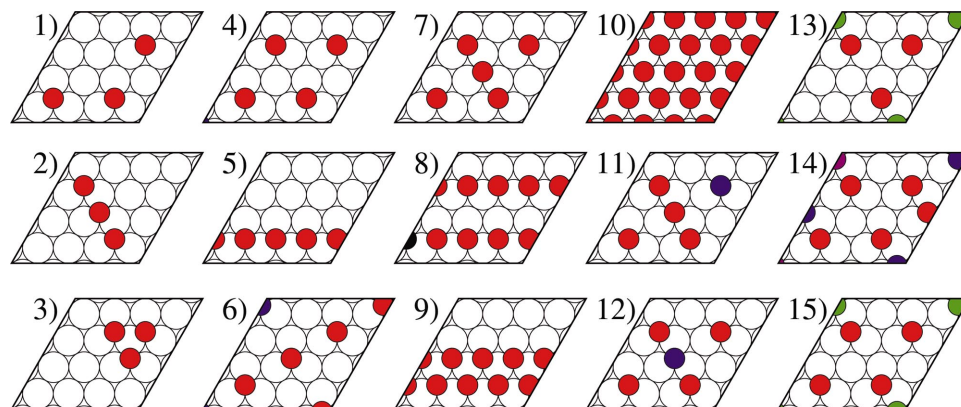


FIG. 2. (Color) Adsorption geometries considered besides those used for the computation of Tables I and II. All adsorption occurs in threefold fcc hollows. The colors red, blue, and green denote  $\text{O}$ ,  $\text{NO}$ , and  $\text{NO}_2$  adsorbates, respectively.

TABLE III. Energies in eV for the adsorbate configurations displayed in Fig. 2. To facilitate comparisons, the zero of the energy scale is set to  $E_0 = m \cdot E_N^1 + n \cdot E_O^1 - (m+n-1)E_{\text{slab}}$ , where  $E_N^1$  ( $E_O^1$ ) is the energy of an isolated N (O) atom adsorbed on a clean slab, and  $m$  ( $n$ ) denotes the number of N (O) ions in the cell, so that  $E_0 = 0$ , if no interactions are present. The energy given is  $E_{\text{int}} = (E - E_0)/(m+n)$ .  $E_{\text{PW}}$  is the value of  $E_{\text{int}}$  predicted, if interactions are pairwise additive and negligible beyond third-nearest-neighbor separation.

No.	$E_{\text{int}}$	$E_{\text{int}} - E_{\text{PW}}$	No.	$E_{\text{int}}$	$E_{\text{int}} - E_{\text{PW}}$
1	0.03	-0.00	9	0.49	-0.03
2	0.15	0.01	10	0.99	0.02
3	0.21	0.00	11	0.10	-0.05
4	0.04	-0.01	12	0.12	-0.01
5	0.25	0.03	13	0.13	0.09
6	0.10	-0.03	14	0.18	-0.05
7	0.14	0.02	15	0.14	0.07
8	0.32	0.07			

formation (1.25 eV),  $\text{NO}_2$  decomposition (0.90 eV), and  $\text{NO}_2$  desorption (1.28 eV).

The most complex reaction in this study is  $\text{NO} + \text{O} \rightarrow \text{NO}_2$ . It starts with an upright N-down NO molecule adsorbed in an fcc site with an oxygen atom in a neighboring fcc site and ends in the  $\mu$ -N,O-nitrito  $\text{NO}_2$  configuration, i.e., with all fragments in their energetically preferred sites. Because of its higher mobility,<sup>15</sup> the reaction proceeds with the NO molecule diffusing towards the adsorbed O atom via a bridge site, as depicted in Fig. 1. As the NO crosses the bridge site and the two fragments are about 2.5 Å away, the adsorbed O atom has already moved about 0.8 Å to accommodate the formation of a chemical bond. We find the activation energy for this process to be about 1.25 eV at low coverage, noting that this value is likely sensitive to the local adsorption environment and that there may be lower-energy reaction pathways.

Coverage effects are accounted for by summing pair interactions in initial and final configurations up to 3-NN separations and then adjusting barrier energies with a simple interpolation formula,<sup>24</sup>

$$E_A = E_A^0 + \frac{1}{2}(E_f - E_i), \quad (1)$$

where  $E_A^0$  is the low-coverage limit of the activation energy, and  $E_f$  and  $E_i$  are the total interaction energies of the final and initial states of the motion, respectively. All prefactors are set to  $10^{13}$  Hz.<sup>25</sup> At high temperatures, adsorbate diffusivities are suppressed by a common factor to reduce CPU time consumption; convergence with respect to this parameter is carefully checked.<sup>26</sup>

For oxygen, the fcc hollow site is preferred by 0.41 eV over the hcp site. We find this preference to increase when the surface is precovered with a  $p(2 \times 2)$  O overlayer, in contrast to a recent thermal desorption study.<sup>27</sup> For NO, the fcc-hcp difference is smaller (0.10 eV), but the NO diffusion is found to be of minor importance for the reaction kinetics. As for  $\text{NO}_2$ , the fact that it does not bind in registry with the

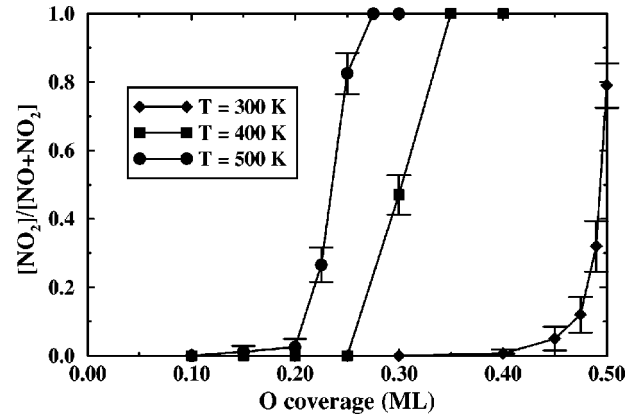


FIG. 3. Efficiency of the NO oxidation process as a function of initial oxygen coverage and temperature on Pt(111). Statistical errors of two standard deviations are indicated.

substrate has little influence on the kinetics, as there is always one fcc site in the proximity of the  $\text{NO}_2$ , where no adsorption is possible, and that site can then be treated as occupied by the  $\text{NO}_2$ .

Hence, in the KMC simulations fcc sites only are considered.

Adsorbates move on a triangular lattice with periodic boundary conditions containing  $40 \times 40$  sites. Oxygen atoms are first deposited at random on the clean surface, and the system is equilibrated for 1 s. With the focus on the dilute limit of NO abundance, exactly one NO molecule is then deposited, and the system is annealed for another 2 s. Within this time  $\text{NO}_2$  may form, decompose, and desorb.

## VII. KINETICS

The computed final fraction of  $\text{NO}_2$  (at the surface and in the gas phase) as a function of temperature and initial oxygen coverage (Fig. 3) shows unexpected features: The NO oxidation reaction turns on at about 0.2 ML O coverage for the highest temperature considered but requires up to 0.25 ML more oxygen at 300 K. This is mainly a kinetic effect, as at 300 K the opposite reaction does not take place for any coverage above 30%. At 0.20 ML O coverage the oxidation reaction does not occur to an appreciable extent for any temperature—as expected from the sample DFT results discussed above—but the enhancement of the reactivity with increasing  $\Theta_{\text{O}}$  is strongly temperature dependent.

Thus, at high temperatures, the reaction can be driven back and forth with slight changes in the O coverage around 0.25 ML, whereas at low temperatures, large changes are required for kinetic reasons. The  $\text{NO}_2$  formation reaction is thus activated by both temperature and the accumulation of O atoms around the NO.

Given the strong sensitivity of the oxidation efficiency to the oxygen coverage, there is good reason to investigate experimentally or theoretically the external conditions for bringing the system slightly above or below the critical coverages.

### VIII. CONCLUDING REMARKS

In conclusion, the  $\text{NO} \rightleftharpoons \text{NO}_2$  reaction on an O-covered Pt(111) substrate is studied using first-principles KMC simulations. The catalytic activity is found to depend strongly on the oxygen coverage. The surface reaction is highly endothermic in the low-coverage limit but turns exothermic at  $\Theta_{\text{O}} \approx 25\%$ , due to repulsive lateral O-O and O-NO interactions. However, for kinetic reasons, as much as 0.45 ML O coverage is required for the reaction to be activated at room

temperature. These findings are congruent with flow-reactor experiments<sup>28</sup> and should encourage future ultra-high-vacuum studies.

### ACKNOWLEDGMENTS

Support from the Swedish Research Council and the Swedish Foundation for Strategic Research via the ATOM-ICS consortium is gratefully acknowledged.

\*Present address: Department of Chemical and Biomolecular Engineering, University of Notre Dame, Notre Dame, Indiana 46556, USA.

<sup>1</sup>M. Shelef and R. W. McCabe, *Catal. Today* **62**, 35 (2000).

<sup>2</sup>V. I. Parvulescu, P. Grange, and B. Delmon, *Catal. Today* **46**, 233 (1998).

<sup>3</sup>N. W. Cant and I. O. Y. Liu, *Catal. Today* **63**, 133 (2000).

<sup>4</sup>N. Takahashi, H. Shinjoh, T. Iijima, T. Suzuki, K. Yamazaki, K. Yokata, H. Suzuki, N. Miyoshi, S. Matsumoto, T. Tanizawa, T. Tanaka, S. Tateishi, and K. Kasahara, *Catal. Today* **27**, 63 (1996).

<sup>5</sup>E. Fridell, M. Skoglundh, B. Westerberg, S. Johansson, and G. Smedler, *J. Catal.* **183**, 196 (1999).

<sup>6</sup>C. Stampfl, H. J. Kreuzer, S. H. Payne, H. Pfnür, and M. Scheffler, *Phys. Rev. Lett.* **83**, 2993 (1999).

<sup>7</sup>W. X. Li, C. Stampfl, and M. Scheffler, *Phys. Rev. B* **65**, 075407 (2002).

<sup>8</sup>A. Bogicevic, S. Ovesson, P. Hyltdgaard, B. I. Lundqvist, H. Brune, and D. R. Jennison, *Phys. Rev. Lett.* **85**, 1910 (2000); S. Ovesson, A. Bogicevic, G. Wahnström, and B. I. Lundqvist, *Phys. Rev. B* **64**, 125423 (2001).

<sup>9</sup>P. Ruggerone, C. Ratsch, and M. Scheffler, in *Growth and Properties of Ultrathin Epitaxial Layers*, edited by D. A. King and D. P. Woodruff (Elsevier Science, Amsterdam, 1997), p. 490.

<sup>10</sup>A. Bogicevic, J. Strömquist, and B. I. Lundqvist, *Phys. Rev. Lett.* **81**, 637 (1998); S. Ovesson, A. Bogicevic, and B. I. Lundqvist, *ibid.* **83**, 2608 (1999).

<sup>11</sup>P. Kratzer and M. Scheffler, *Phys. Rev. Lett.* **88**, 036102 (2002).

<sup>12</sup>A possible exception is the hydrocarbon/Pt(111) system [E. W. Hansen and M. Neurock, *J. Catal.* **196**, 241 (2000)]. However, in that study, the reaction energetics is taken from DF calculations based on small model clusters of the metal surface, which generally lack the accuracy needed for predictive KMC simulation.

<sup>13</sup>J. P. Perdew, in *Electronic Structure of Solids*, edited by P. Ziesche and H. Eschrig (Akademie Verlag, Berlin, 1991), Vol. 11.

<sup>14</sup>The accuracy of PW91 for molecular adsorption systems is discussed in B. Hammer, L. B. Hansen, and J. K. Nørskov, *Phys.*

*Rev. B* **59**, 7413 (1999).

<sup>15</sup>A. Bogicevic and K. C. Hass, *Surf. Sci.* **506**, L237 (2002).

<sup>16</sup>H. Jónsson, G. Mills, and K. W. Jacobsen, in *Classical and Quantum Dynamics in Condensed Phase Simulations*, edited by B. J. Berne, G. Ciccotti, and D. F. Coker (World Scientific, Singapore, 1998).

<sup>17</sup>W. X. Huang and J. M. White, *Surf. Sci.* **529**, 455 (2003).

<sup>18</sup>M. E. Bartram, R. G. Windham, and B. E. Koel, *Surf. Sci.* **184**, 57 (1987).

<sup>19</sup>C. Ratsch and M. Scheffler, *Phys. Rev. B* **58**, 13 163 (1998).

<sup>20</sup>M. Kaburagi and J. Kanamori, *J. Phys. Soc. Jpn.* **44**, 718 (1978).

<sup>21</sup>B. C. Stipe, M. A. Rezaei, and W. Ho, *J. Chem. Phys.* **107**, 6443 (1997).

<sup>22</sup>J. Winterlin, R. Schuster, and G. Ertl, *Phys. Rev. Lett.* **77**, 123 (1996).

<sup>23</sup>A. F. Voter, *Phys. Rev. B* **34**, 6819 (1986).

<sup>24</sup>K. A. Fichthorn and M. Scheffler, *Phys. Rev. Lett.* **84**, 5371 (2000). On this level of complexity, applying this formula is the best that one can do because (i) it ensures that energy is conserved and always amounts to the total pairwise added interaction energy, (ii) it is the only simple choice that introduces no asymmetry between initial and final states of a reaction, and (iii) any inaccuracy in reaction rates brought with it is mitigated by a compensating higher or lower rate in the opposite direction.

<sup>25</sup>The prefactor generally approximates to this “universal” value [see V. P. Zhdanov, *Surf. Sci. Rep.* **12**, 183 (1991) and R. Gomer, *Rep. Prog. Phys.* **53**, 917 (1990)], give or take an order of magnitude, the precise value usually being of little significance, as the total rate depends much more strongly on the activation energy, which enters in the exponential. Such values are also obtained in DFT calculations (Ref. 19).

<sup>26</sup>The suppression factors were decreased in steps of an order of magnitude until the results in Fig. 3 did not change significantly.

<sup>27</sup>D. I. Jerdev, J. Kim, M. Batzill, and B. E. Koel, *Surf. Sci.* **498**, L91 (2002).

<sup>28</sup>L. Olsson, H. Persson, E. Fridell, M. Skoglundh, and B. Andersson, *J. Phys. Chem. B* **105**, 6895 (2001).